

Star formation and bar instability in cosmological haloes

Anna Curir,¹ Paola Mazzei² and Giuseppe Murante¹

¹ INAF-Osservatorio Astronomico di Torino, Strada Osservatorio 20 -10025 Pino Torinese (Torino), Italy. e-mail:curir@to.astro.it

² INAF-Osservatorio Astronomico di Padova, Vicolo Osservatorio 5 - 35122 Padova, Italy

ABSTRACT

Context. This is the third of a series of papers presenting the first attempt to analyze the growth of the bar instability in a consistent cosmological scenario. In the previous two articles we explored the role of the cosmology on stellar disks, and the impact of the gaseous component on a disk embedded in a cosmological dark matter halo.

Aims. The aim of this paper is to point out the impact of the star formation on the bar instability inside disks having different gas fractions.

Methods. We perform cosmological simulations of the same disk-to-halo mass systems as in the previous works where the star formation was not triggered. We compare the results of the new simulations with the previous ones to investigate the effect of the star formation by analysing the morphology of the stellar components, the bar strength, the behaviour of the pattern speed. We follow the gas and the central mass concentration during the evolution and their impact on the bar strength.

Results. In all our cosmological simulations a stellar bar, lasting 10 Gyr, is still living at $z=0$.

The central mass concentration of gas and of the new stars has a mild action on the ellipticity of the bar but is not able to destroy it; at $z=0$ the stellar bar strength is enhanced by the star formation. The bar pattern speed is decreasing with the disk evolution.

Key words. galaxies: spirals, structure, evolution, halos, kinematics and dynamics

1. Introduction

The connection between the bar feature and the star formation process has already been pointed out in the past: Martinet & Friedli (1997) observed that non interacting galaxies displaying the highest star forming activity have strong and long bars. Conversely not all strong and long bars are intensively creating stars. Mazzei & Curir (2001) performed SPH simulations to investigate the dependence of the star formation in disks on the geometry and dynamical state of the DM halo. They showed that the star formation lengthens the life time of the bar. However in their works the evolution of the disk+halo system arises in a isolated framework, outside the cosmological scenario.

The treatment of the star formation in galaxies involves a large number of physical processes which arise with different time scales and spatial lengths. Therefore its inclusions in simulations of galaxy formation is complex (Mazzei & Curir (2003) and references therein) and many sub-grid parametrisations (i.e. representing all the astrophysical processes that cannot be resolved due to resolution or computing power limitations) of the star formation process, exist in literature. To mimic all these processes with a numerical model of a realistic disk galaxy is difficult too. Thus the numerical work on this subject focuses either on a detailed analysis of the interstellar medium (ISM) and a smaller simulated area (Wada 2001; Avillez et al. 2000) or on the study of the global instabilities and of the star formation at the cost of simplified ISM models (Robertson et al. 2004; Semelin & Combes 2002; Combes & Melchior 2002). Models that have tackled both topics have either been in two dimensions (Wada & Norman 2001) or restricted to a box size a few hundred parsecs across (Wada 2001). Rosen & Bregman (1995) worked in two dimensions allowing the ISM to evolve self-consistently but treated the stars as collisional rather than col-

lisionless fluid. Tasker & Bryan (2006) presented the first three dimensional simulations of a global disk without the need to simplify the structure of the ISM. Their paper is devoted to understand the fundamental processes of star formation and feedback in a disk galaxy.

Here we performed cosmological simulations to analyse the effects of the star formation process inside stellar-gaseous disks embedded in a DM cosmological halo evolving in a fully consistent scenario. We employ the sub-grid star formation model by Springel & Hernquist (2003) which is able to produce a self-regulated star formation in galactic disks. We point out that our model is not a general galaxy evolution model, since the gradual formation and growth of the stellar disk has not been taken into account. However our approach, developed in two previous papers (Curir et al. 2006, 2007), allows us to investigate the effects of different parameters like the disk-to-halo mass ratio and the gas fraction inside the disk, on the growth of the bar instability, its coupling with the star formation rate and its dependence on such parameters in a self-consistent cosmological framework. We compare the results of such a new set of simulations with those of our previous sets with the star formation switched off (Curir et al. (2006), hereafter Paper 1, Curir et al. (2007), hereafter Paper 2). In Paper 1 we presented simulations of purely stellar disks with the same disk-to-halo mass ratios, in the same cosmological scenario, and with the same initial conditions as in this new paper. In Paper 2 we investigated the growth and the evolution of the bar instability in disks with the same disk-to-halo mass ratios as in Paper 1, and different gas fractions, without star formation. Thus, we will compare the results of simulations here performed, with those corresponding to the same disk-to-halo mass ratio as in Paper 1 and to the same gas fraction as in Paper 2. The comparison between the parameters characterising the bar can be done only evaluating that of the old stars component, since the new stars are not present in Paper 1

and 2. In both such Papers it was shown that in DM dominated disks a bar feature is triggered and maintained by the Cosmology whereas, in the more massive disks, a gas fraction 0.2 is able to destroy the bar. The focus of the present work is to determine if the star formation changes such a result.

The plan of the paper is the following: in Section 2, we summarise our recipe for the initial *disk+halo* system fully described in Paper 1, and present our star formation recipe. In Section 3 there are our cosmological simulations, in Section 4 we point out our results. The parameters related to the bars formed in the new and the old stars and to the global, old+new, stellar populations are given in such a section. Section 5 is devoted to our discussion and conclusions. It contains a Table including the parameters characterising the old stellar bar at $z=0$ in the three Papers to allow a more easy comparison between the results of our Papers (Table 2).

2. Method

We embed a gaseous and stellar disk inside a cosmological halo selected in a suitable slice of Universe and follow its evolution inside a cosmological framework: a Λ CDM model with $\Omega_m = 0.3$, $\Omega_\Lambda = 0.7$, $\sigma_8 = 0.9$, $h = 0.7$, where Ω_m is the total matter of the Universe, Ω_Λ the cosmological constant, σ_8 the normalisation of the power spectrum, and h the value of the Hubble constant in units of $100h^{-1} \text{ km s}^{-1} \text{ Mpc}^{-1}$.

A detailed description of our method to produce the cosmological scenario where the disk is evolved has been given in Paper 1. Here we present a short overview of our recipe. Paper 1 showed that the numerical resolution does not impair their main result: in pure stellar disks, long living bars are a 'natural' outcome of the cosmological scenario.

2.1. The DM halo

To select the DM halo, we perform a low-resolution simulation of a *concordance* Λ CDM cosmological model, starting from redshift 20.

With a standard 'friends of friends algorithm' we selected one suitable DM halo with a mass $M \sim 10^{11} h^{-1} M_\odot$ (at $z=0$). We resample it with the multi-mass technique described in Klypin et al. (2001). The particles of the DM halo, and those belonging to a sphere with a radius $4h^{-1} \text{ Mpc}$, are followed to their Lagrangian position and re-sampled to an equivalent resolution of 1024^3 particles. The total number of DM particles in the high resolution corresponds to a DM mass resolution of $1.21 \cdot 10^6 h^{-1} M_\odot$. The high-resolution DM halo is followed to the redshift $z=0$. We run the DM simulation, to extract the halo properties in absence of any embedded stellar disk. The mass of our halo at $z=0$, $1.03 \cdot 10^{11} h^{-1} M_\odot$, corresponds to a radius, $R_{vir} = 94.7 h^{-1} \text{ Kpc}$, which entails 84720 halo particles. The selected halo is living in an under-dense environment. From its accretion history (see Fig. 1 in Paper 1) we conclude that our halo undergoes no significant merger during the time it hosts our disk, nor immediately before. The halo density profile is well-fitted by a Navarro, Frenk and White (NFW) form (Navarro et al. (1996); Navarro et al. (1997)) at $z \leq 2$. The concentration, C_{vir} , equal to R_{vir}/R_s , takes an high value, 18.1, confirming that this halo does "form" at quite high redshift (e.g. Wechsler et al. (2002) for a discussion about the link between concentration and assembly history of the halo). The dimensionless spin parameter of the halo is 0.04 at $z=2$, near to the average one for our cosmological model (Maller et al. 2002; Bett et al. 2007).

Cosmological DM haloes are not spherical (Bett et al. 2007, and

references therein). From a recent analysis of the halo shapes from the Millennium simulation, Bett et al. (2007) show that haloes are triaxial and prolate. Their shape is driven by the hierarchical formation. The prolateness of our halo at $z=2$, where $R_{vir} = 30 \text{ Kpc}$, is 0.9, quite the same as at the disk radius (Paper 1, Table 1).

2.2. The baryonic disk

The spatial distribution of particles follows the exponential surface density law: $\rho = \rho_0 \exp(-(r/r_0))$ where r_0 is the disk scale length, $r_0 = 4h^{-1} \text{ Kpc}$, and ρ_0 is the surface central density. The disk is truncated at five scale lengths with a radius: $R_{disk} = 20h^{-1} \text{ Kpc}$. To obtain each disk particle's position according to the assumed density distribution, we used the rejection method (Press et al. 1986). We used 56000 star particles and 56000 gaseous particles to describe our disk. The (Plummer equivalent) softening length, the same for DM, gas, and star particles, is $0.5h^{-1} \text{ Kpc}$ in comoving coordinates.

We embed the disk in the high resolution cosmological simulation, at redshift 2, in a plane perpendicular to the angular momentum vector of the halo and in gravitational equilibrium with the potential. Its centre of mass corresponds to the minimum potential well of the DM halo. The initial redshift corresponds to 10.24 Gyr down to $z=0$ in our chosen cosmology. During the evolution, new star particles are formed from the gaseous particles. We will refer to such new component as 'new stars component', whereas we will call 'old stars component' the non dissipative particles present in the disks at $z=2$.

2.3. Star formation recipe

We use the sub-grid star formation prescription by Springel & Hernquist (2003). In such prescription, when a gas particle overcomes a given density threshold its gas content is considered to reside in a multi-phase state, corresponding to the equilibrium solution of an analytical model describing the physics of the multi-phase interstellar medium. Such a solution gives an effective temperature for the gas particle, obtained as a weighted average of the (fixed) temperature of the cold phase and that of the hot phase. The temperature of the hot phase is set by supernova feedback and by the efficiency of cloud evaporation. The resulting inter stellar medium (ISM) has an effective equation of state $P_{eff}(\rho)$ which is stiffer than isothermal and prevent Toomre instabilities even when a large amount of gas is present. When this prescription is used, the star formation rate agrees with the Schmidt law in disk galaxies, as obtained e.g. by Kennicutt (1998). A detailed description of the numerical prescription and several tests can be found in Springel & Hernquist (2003). The effective temperature drives hydrodynamical interactions of the gas particles. Moreover, the model consistently gives a star formation rate, which is used to spawn a star particle from the gas one on the basis of a stochastic prescription; the initial mass function adopted is the Salpeter's one. The star forming from the gas has the same position and velocity of the gaseous particle.

3. Simulations

We performed six cosmological simulations of a disk+halo system. We exploited the parallel Tree+SPH N-body code GADGET-2 (Springel 2005) (courtesy of V. Springel). The simulations run on the CLX computers located at the CINECA com-

Table 1. Simulations: final values. o.s.=old stars , n.s.= new stars

N	M_{disk}	gas fraction	ϵ (o.s.)	ϵ (n.s.)	Q_b (o.s.)	Q_b (o.s.+n.s.)	a_{max} (o.s.)	a_{max} (n.s.)	bulge(o.s.)	bulge(n.s.)	bars in bars
c1	0.33	0.1	0.65	0.72	0.45	0.5	8	4	y	n	n
c2	0.33	0.2	0.55	0.55	0.51	0.66	11	5.7	y	y	n
c3	0.33	0.4	0.6	0.55	0.58	0.69	8.4	6	y	y	n
c4	0.1	0.1	0.39	0.01	0.5	0.41	3	-	n	y	y
c5	0.1	0.2	0.45	0.03	0.46	0.42	3	-	n	y	y
c6	0.1	0.6	0.5	0.02	0.51	0.47	3	-	n	y	y

puting center (BO, Italy) and on OATo Beowulf-class cluster of 32 Linux-based PC at the Osservatorio Astronomico di Torino. The main parameters and the final properties of our set of simulations are listed in Table 1. We define as a geometrical measure of the bar strength the value of the ellipticity, $\epsilon = 1 - b/a$ (Table 1); a strong bar corresponds to $\epsilon \geq 0.4$. A more dynamical measure of the bar strength at radius R has been defined by Combes & Sanders (1981) by using the parameter: $Q_t = \frac{F_T^{max}(R)}{\langle F_R(R) \rangle}$ where $F_T^{max}(R) = [\partial\Phi(R, \theta)/\partial\theta]_{max}$ is the maximum amplitude of tangential force and $\langle F_R(R) \rangle = R(\partial\Phi_0/\partial r)$ is the mean axisymmetric radial force derived from the $m = 0$ component of the gravitational potential at the same radius, R. The maximum value of $Q_t(R)$ provides a measure of the bar strength Q_b for the whole galaxy. Stronger bars correspond to higher Q_b values. In order to compare the results with the Papers 1 and 2 the values of Q_b are evaluated in the bars formed in the old stars component, since in our previous works we didn't include the star formation process.

We give here in Table 1 also the value of the parameters related to the bars formed in the new stars component and to the bar strength of the global old+new stars populations. In Table 1 we present: the simulation number (I column), the mass of the disk in code units (i. e. $5.9 \times 10^{10} M_\odot$) (II col.), the fraction of gas, i.e. gas-to-disk mass ratio (III col.). Moreover we present, as final values (i. e. at $z = 0$) the maximum ellipticity for the old stars system (IV col.), and for the new stars (V col.) the bar strength according to Combes & Sanders (1981) for the old stars (VI col.), and for the old+new stars system (VII col.), the major axis (physical Kpc) corresponding to the maximum ellipticity for the old stars (VIII col.) and for the new ones (IX col.), the morphology of the inner region of the disk for the old stars (X col.) and for the new ones (XI col.), peculiar features inside the disk (XII col.).

4. Results

In all our cosmological simulations, a stellar bar is still living at $z=0$ in the old star component. The new stars component at $z=0$ is arranged in a bulge component which can or cannot present a barred shape depending on the initial mass of the disk and on the gaseous fraction.

In Figs 1-8 we present the isodensity contours of the old stars, gas and new stars for simulations in Table 1. All such figures have been built up with the same box-size, number of levels, and density contrast (see caption of Fig. 1), as in Papers 1 and 2.

4.1. Morphologies

We will discuss first the bar features as far as the old star component is concerned. Fig.1 and Fig.2 show the evolution of this component from $z=2$ to $z=0$ for simulation c1 and c4. The bar feature is well defined since $z=1.75$ in both the cases. In the more

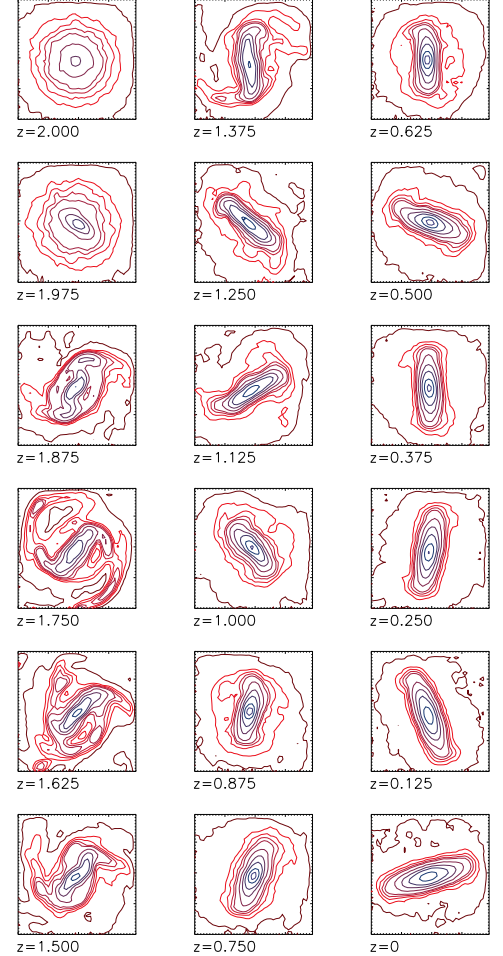


Fig. 1. Face-on isodensity contours of simulation c1 from $z=2$ to $z=0$. Spatial resolution is always $0.5h^{-1}$ physical Kpc and the box size is 40 times the spatial resolution. Contours are computed at 11 fixed levels ranging from 2×10^{-4} to 0.015 in term of density fraction of stars (gas) within the spatial resolution to the total star (gas) density in the map.

massive case, the evolving bar becomes stronger and dominates the disk, whereas in the less massive case, the bar remains a central structure inside the disk, generating a bar-in-bar feature. The strongest bar arises from simulation c1 (Fig. 3). In this case, the ellipticity, evaluated through the isodensity plots, is higher (0.65) than the one measured in the purely stellar disk of the same mass (0.52, Paper 1), but slightly smaller than that measured in the case of a disk with the same mass and the same gas fraction (0.68, Paper 2). The enhancement of the stellar bar strength in comparison to the gas free case is due to the coupling of the gaseous component to the stellar one: the gaseous bar is indeed superimposed to the stellar one, as pointed out in Paper

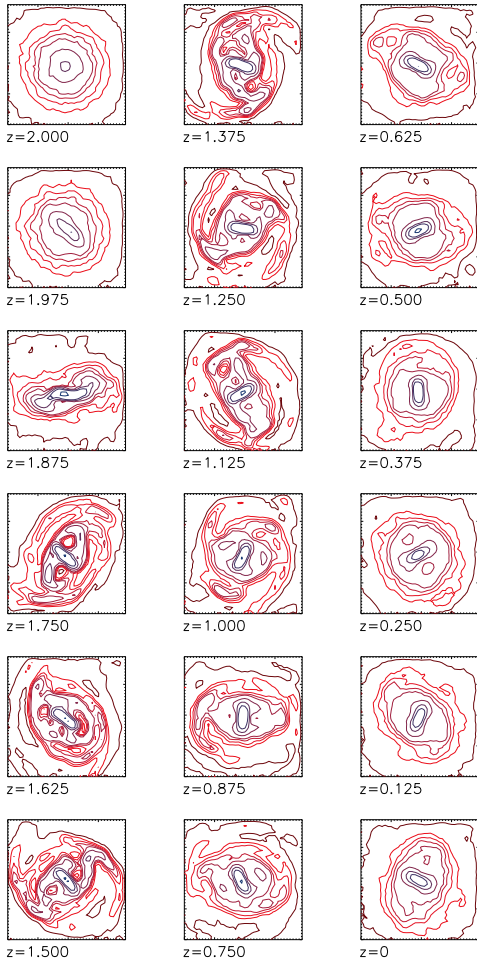


Fig. 2. Face-on isodensity contours of simulation c4 from $z=2$ to $z=0$. Isodensity levels and spatial resolution are the same as in Fig. 1

2. However, this effect is slightly reduced by the star formation activity.

In the simulation c2, the stars produce a barred feature, lasting until $z = 0$ (Fig. 4). This is an important difference with the case having the same gas fraction in Paper 2, where the bar was decreasing its strength and disappearing at $z \approx 0.15$. The same behaviour arises also in the c3 case (Fig. 5), which corresponds to a larger initial gas fraction: the bar is living until the final redshift, whereas, without the star formation, the bar was disappearing at $z \approx 0.6$.

The gas forms a bar since the beginning of the disk evolution and the new stars originating from the gaseous component assume an elongated structure which fuels the old stars bar feature: the new stars are dynamically cold and they strongly feel the resonances in the equatorial plane, where they are born. In the simulations with higher gas fractions, they are swept out in the central regions by vertical resonances which results in the formation of a central young bulge (Friedli & Benz 1995). According to the claim of Berentzen et al. (1998), the growth of a gas mass concentration in the disk dissolves the regular orbits in the stellar bar. In Paper 2, we deduced a threshold value for the gas concentration inside a radius of 2 Kpc, 9%, able to destroy the bar in the more massive disks. If the star formation is included, it transforms the dissipative component into a non dissipative one and therefore the central concentration of the gas is lower. Fig.

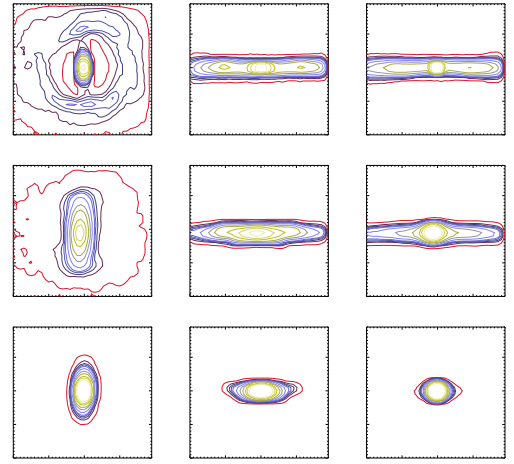


Fig. 3. Face-on, edge-on and side-on isodensity contours (from left to right) of simulation c1 at $z=0$ (see text); top panel shows the gaseous component, middle panel the old star component, bottom panel the new formed stars. Isodensity levels and spatial resolution for gas and stars are as in Fig. 1.

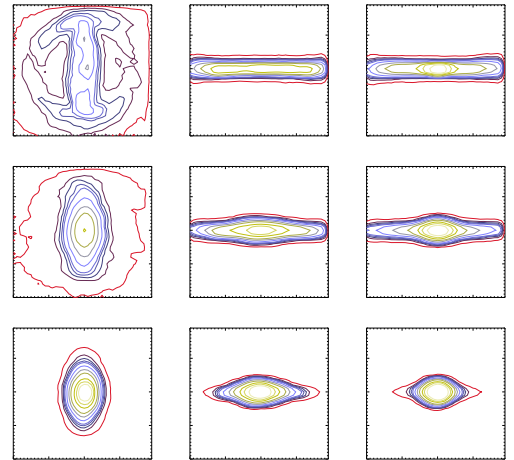


Fig. 4. Same as in Fig. 3 but for simulation c2

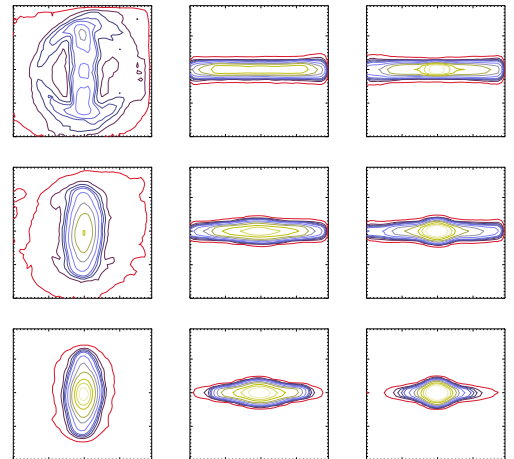


Fig. 5. Same as in Fig. 3 but for simulation c3

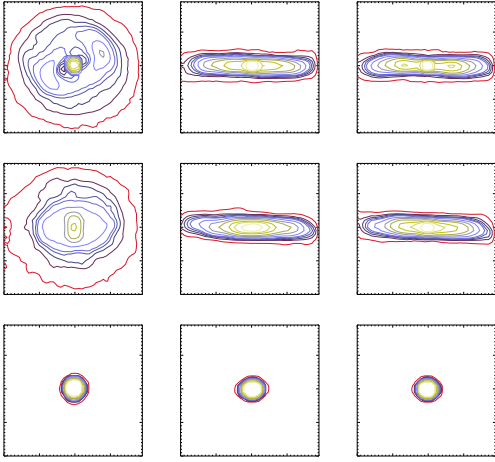


Fig. 6. Same as in Fig. 3 but for simulation c4

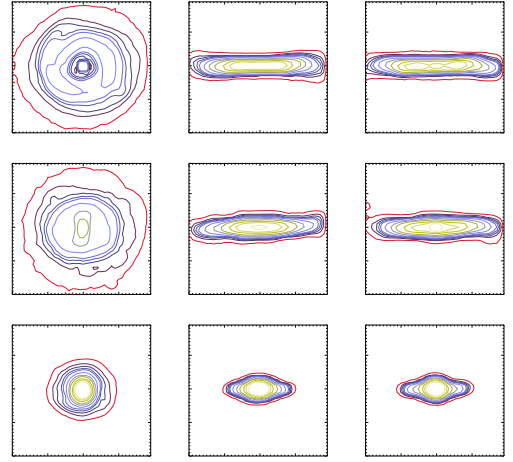


Fig. 8. As in Fig. 3 for simulation c6.

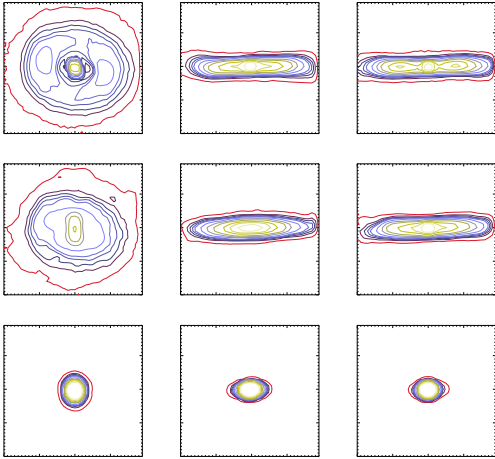


Fig. 7. As in Fig. 3 for simulation c5.

9 and Fig. 10 show the evolution of the gas mass in the inner regions, i.e., of the gas concentration (upper panel), and that of the mass of gas plus new stars (lower panel) in the same regions, in simulations c2 and c3 respectively. In both these cases, the gas mass inside 2 kpc never overcomes the threshold value pointed out in Paper 2. However, the gas+new star concentration in simulation c3 overcomes this threshold value at $z=0.6$, without any consequence on the bar observed (Fig. 11). This is because the effect of bar dissolution due to the central mass concentration cannot be achieved including the mass of new stars which are crossing the central region through elongated orbits and are not really concentrated as the gas. In the simulation c3 the gas shows more developed arms at $z=1$ than in the case c1 (Fig. 12). But this feature, which is considered as a possible mechanism for the bar destruction has no impact on the bar in these new simulations (Bournaud et al. 2005).

A different discussion is devoted to the DM-dominated disks, which, as we already stressed in Paper 1 and 2, show bars which are not a classical product of the self-gravity or of angular momentum exchanges, but they are features that strongly depend on the dynamical state and evolution of the cosmological halo, and we did not observe their destruction even by an higher gas concentration. Old stars in simulation c4 show a stellar bar stronger

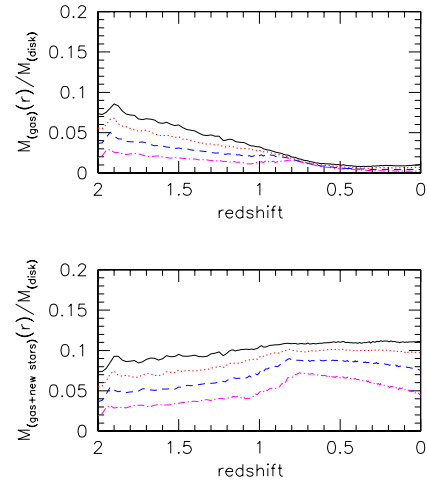


Fig. 9. Gas-to-disk mass ratio at different disk radii : 2 Kpc (magenta dashed-dotted line), 3 Kpc (blue dashed line), 4 Kpc (red dotted line), 5 Kpc (black full line) for simulation c2. In the upper panel we present the time behaviour of the gas as fraction of the disk mass, in the lower panel we see the same for the sum of the gas and the new formed stars.

than that in the pure stellar disk of the same mass (ellipticity 0.39 instead of 0.3, see Tab. 2) but weaker than that arising from the simulation with the same disk mass and gas fraction but without star formation (Paper 2). Bar-in-bar features are present along the whole evolution (simulation c4) until $z=0$ (Fig. 6). Simulations c5 and c6, which correspond to increasing gas fractions, show similar features during the system evolution. In this set of DM dominated disk simulations, the final bar is increasing its strength with the increasing gas fraction (Fig. 13, Tab. 1). This trend is different from the one we observed in Paper 2, where the increasing gas fraction produces an increase to a maximum and then a decrease of the bar strength.

In DM dominated disks the bars in the old star component are the imprint of the halo cosmological properties, as discussed in the previous Papers. Fig. 14, shows the isodensity contours of the halo in the plane of disk in the same frame, with the same

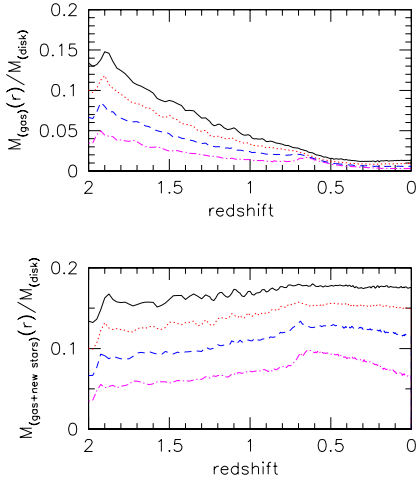


Fig. 10. Same as in Fig. 9 but for simulation c3.

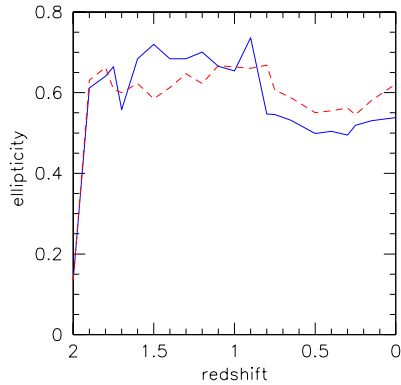


Fig. 11. Evolution in redshift of the ellipticity for simulations c2 (blue full line) and c3 (red dashed line).

isodensity levels, and box sizes as those of the old stars in Fig. 1 and Fig. 2. The semimajor axis of the triaxial DM halo, for $z < 1.8$ is both in phase with the central bar of the disk and they have the same pattern speed.

In the more massive disks (Fig. 15), the central DM region becomes more round, due to impact of the disk itself, and the coupling with the stellar bar disappears. Therefore, in the case of the lighter disks, the cosmological halo properties drive the formation of the bar, whereas in the more massive disks, the bar is a classical product of the disk instability. In the DM dominated disks the new stellar component produces a small spheroidal bulge which has a disky shape in the simulation c6. The gas component is confined in the central regions from the beginning of the evolution, and therefore the new stellar component arranges itself in a small spheroidal bulge. Therefore, in DM dominated disk, the new stars at $z=0$ have no bar features, at difference with more massive disks. We recall that, in DM dominated disks the bars are not due to classical resonances. So, the new stars do not feel these resonances whereas this is what happens in the cases

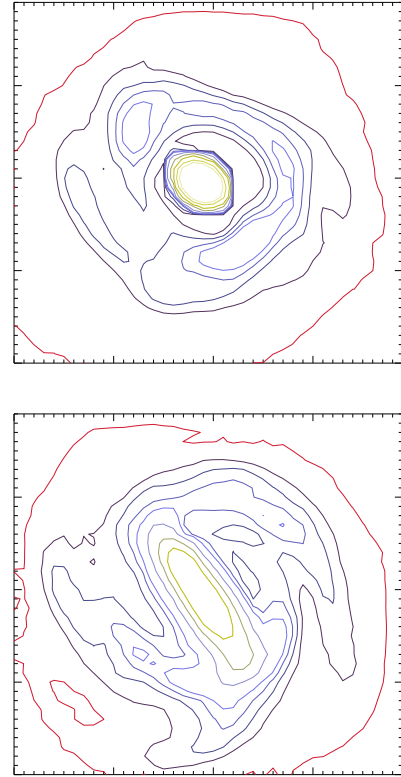


Fig. 12. Gas morphologies at $z=1$ for simulations c1 (left panel) and c3 (right panel).

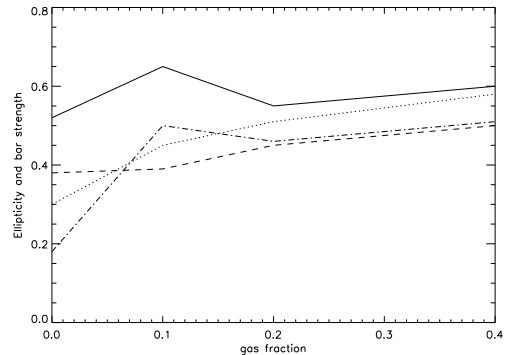


Fig. 13. Behaviour of the bar strength and ellipticity at $z=0$ for our set of cosmological simulations with increasing gas fraction. Q_b (dotted line) and ellipticity (full line) of our more massive disks (i.e. disk-to-halo mass ratio 0.33); Q_b (dot-dashed line) and ellipticity (dashed line) of our less massive, DM-dominated, disks (i.e. disk-to-halo mass ratio 0.1).

of the more massive disks. The decoupling between new and old stars is depicted also by In Fig. 17 the distribution of radial velocity dispersions in a massive disk at $z=1$ is compared with the one in a DM dominated disk at the same redshift; in such a case the decoupling between new and old stars is well depicted. The radial velocity dispersion of this new star component is lower than that of the old stars. At the end of the evolution we therefore see a small bulge of new stars hiding a small nuclear bar of old stars. Such a nuclear bar remains, as observed in Papers 1

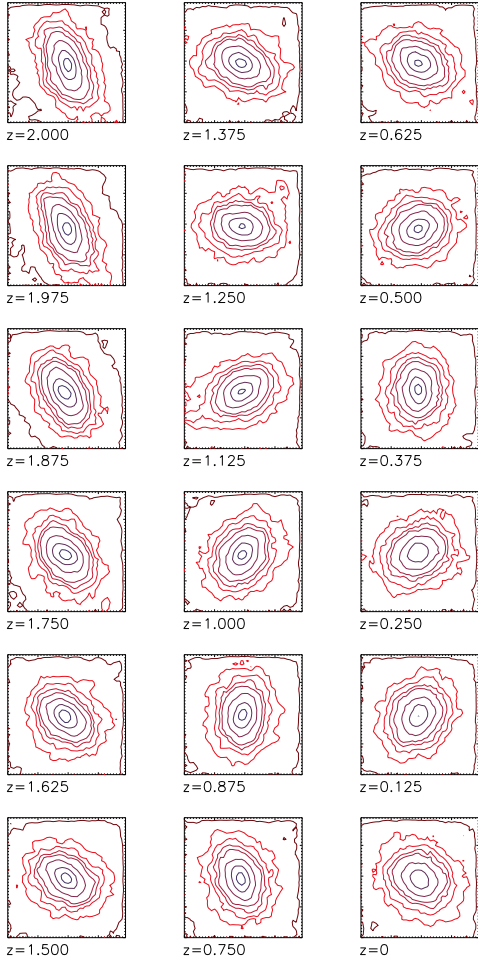


Fig. 14. Isodensity contours of the DM in the xy plane, from redshift $z = 2$ to $z = 0$ for the simulation *c4*. Density levels and spatial resolutions are the same as in Fig. 1. The synchronicity of the semimajor axis of the halo with the one of the inner old stellar bar can be noticed by direct comparison of each panel (after $z=1.8$) with the corresponding one in Fig. 2.

and 2 and stressed by Fig. 14, as a genuine product of the cosmology, since the light disks are classically below the instability threshold.

4.2. Bar pattern speed

The bar pattern speed, Ω_p is the angular speed of the bar-like density wave as viewed from an inertial frame. Here, it is evaluated following the position angle of the major bar axis during the disk evolution, where the major axis is selected with the same criterium E1 quoted in Michel-Dansac & Wozniak (2006), namely as the radius where the ellipticity profile reaches a maximum as in Paper 2. The values of Ω_p as function of the redshift for the more massive disks and the lighter disks are shown in Fig. 18 and Fig. 19 respectively.

For the more massive disks, we observe a decrease of Ω_p in all the simulations. This is a different behaviour from the one observed in Paper 2: there we noticed an increase of the pattern speed coupled with the increasing gas fraction, since the gas presence both shortens the bar and decreases its ellipticity.

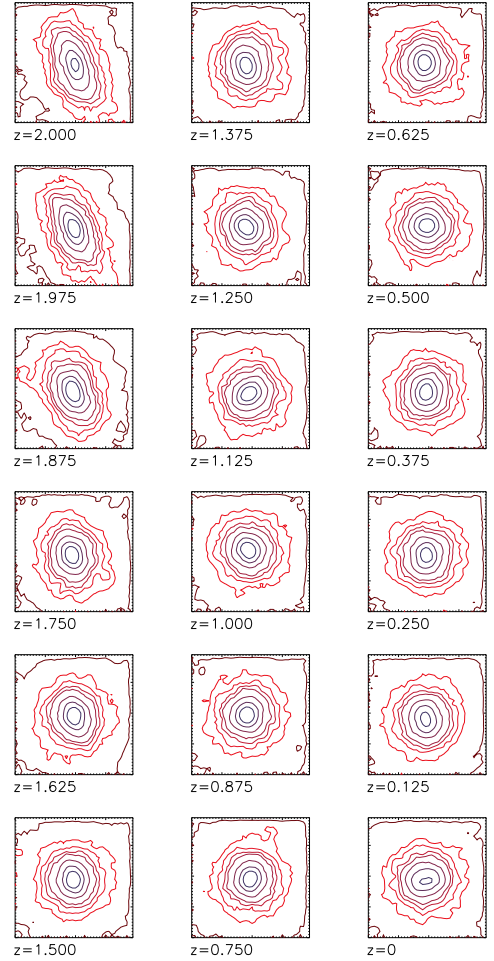


Fig. 15. Isodensity contours of the DM, as in the previous figure, for the simulation *c1*.

This mechanism is no longer working when the star formation is activated, since the ongoing star formation reduces the gas concentration in the central regions and the new stars arrange into an elongated structure which enforces also the length of the original bar (Fig. 20, see also the previous section).

For the DM dominated disks the evaluation of Ω_p in this paper as in the previous ones, is done by referring to the angular velocity of the long-lived central bar. Its behaviour is the same as observed in Paper 2, namely it shows a fast decrease before redshift $z \simeq 1$, and then a quasi stationary behaviour until redshift 0.

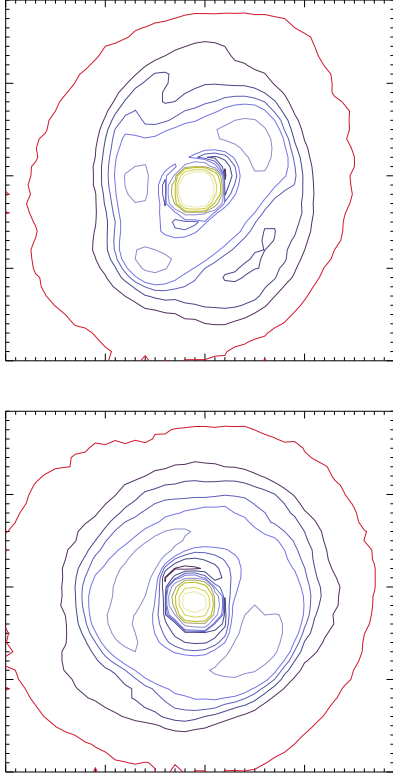
5. Discussion and conclusions

We presented six cosmological simulations with the same disk-to-halo mass ratios as in Paper 1 and Paper 2. In order to study the impact of the forming stars from the gaseous component, here we included and varied its percentages inside disks of different disk-to-halo mass ratios, as in Paper 2 where the star formation was switched off. In Table 2 we show the final data for ellipticities and semimajor axes resuming the results of our three papers.

The old star component show a long lasting bar, 10 Gyr old, in all the simulations of this work. Moreover, in all such simulations, except for simulation *c6*, the bar is stronger than that de-

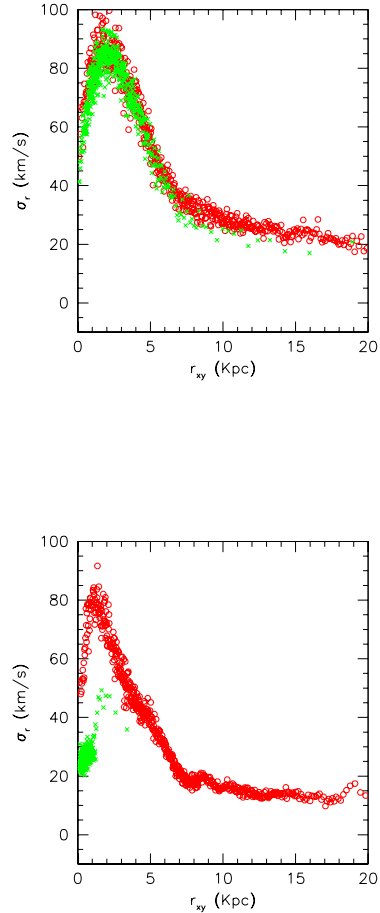
Table 2. Cosmological disks simulations: global results

Disk mass	gas fraction	no star formation		star formation	
		ellipticity	a_{max}	ellipticity	a_{max}
0.33	0.	0.52	5	-	-
0.33	0.1	0.68	8.4	0.65	8
0.33	0.2	0.1	no bar	0.55	11
0.33	0.4	0.07	no bar	0.6	8.4
0.1	0.	0.3	6.5	-	-
0.1	0.1	0.58	5.8	0.39	3
0.1	0.2	0.6	5.4	0.45	3
0.1	0.6	0.42	5.8	0.5	3

**Fig. 16.** Same as in Fig. 12 but for simulations c4 and c6.

veloped in the pure stellar case with the same disk-to-halo mass ratio but weaker than that formed in the case of the same gas fraction without star formation.

We find that the star formation, reducing the central gaseous mass concentration, allows the bar to survive until the end of the evolution also in the more massive disks, at variance with the results in Paper 2 (where the gas was not allowed to form stars): in such a case a gas fraction 0.2 was able to destroy the bar. Even if some details of the disk morphologies obviously depend on the star formation prescription, the bars arising here in the c2 and c3 simulations are due to the reduced central gas concentration and thus to the weakening of its effect on the bar itself. We verified this point by rerunning simulation c2 changing the star formation prescription. Instead of the GADGET-2 effective model, we used a simple algorithm in which, when a gas particle reaches a given density threshold with a temperature lower than a minimum temperature threshold, it is converted into a star particle, as in Katz et al. (1996). Fig. 21 shows the morphology of the old

**Fig. 17.** Radial velocity dispersion at $z=1$ of old stars (red open circles) and new stars (green crosses) for simulations c2 (left panel) and c5 (right panel).

stellar component for such a different star formation recipe: the survival of the bar is due to the star formation, independently on its details.

In all the simulations of more massive disks, the new stellar component shows a barred shape coupled with that of old stars but with semimajor axis and ellipticity values smaller than those. In all the simulations of DM dominated disks, a bar feature is maintained in the old stellar component at the disk center, and the new stars form a spheroidal bulge that hides the bar of the old stars.

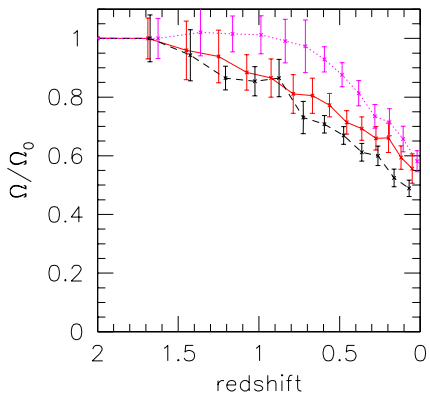


Fig. 18. Evolution of the bar pattern speed with the redshift for simulation c1 (black dashed line), c2 (red full line) and c3 (magenta dotted line).

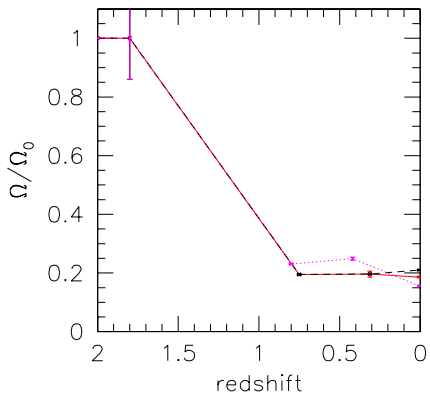


Fig. 19. Evolution of the bar pattern speed with the redshift for simulation c4 (black dashed line), c5 (red full line) and c6 (magenta dotted line).

This effect could be of interest as far as the observations about the Milky Way are concerned where, in addition to the main bar, a small nuclear bar consisting of old stars seems to be included in the bulge (see e. g. Alard (2001)).

The final strength of these old star bars increases by increasing gas fraction and their pattern speed is quickly decreasing before $z=1$.

The classical results obtained outside the cosmological scenario are no longer applicable. This conclusion remarks the results of Paper 1, where it was shown that in the DM dominated disks the bar feature is triggered and maintained by the cosmological properties of the halo (namely its triaxiality and its dynamical state).

From the models presented here we suggest that a very low pattern speed (few $Km s^{-1} Kpc^{-1}$) could be a signature of a dominating halo and not a classical product of the disk instability.

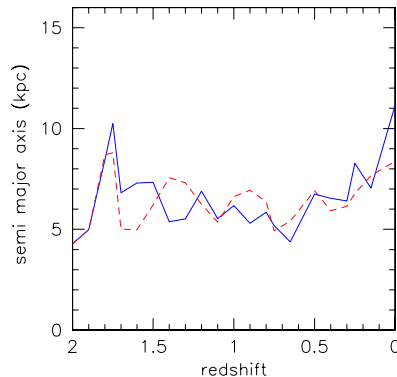


Fig. 20. Behaviour of the semimajor axis for the simulations c2 (blue full line) and c3 (red dashed line).

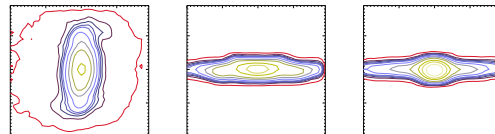


Fig. 21. Isodensity contours of the old stars at $z=0$, for the simulation c2, rerun with the Katz'96 star formation recipe

The whole set of cosmological simulations we presented here is suggesting that the star formation works in favour of maintaining the bar feature in self gravitating disks, against the effect of increasing gas fractions, whereas in DM dominated disks, it slightly reduces the bar strength. Moreover, inside such disks, the new stars are arranged in non barred systems which are decoupled from the bar of the old star component.

Acknowledgements Simulations have been performed on the CINECA IBM CLX Cluster, thanks to the INAF-CINECA grants cnato43a/inato003 “Evolution of disks in cosmological contexts: effect of the star formation inside the disk”, and on the Linux PC Cluster of the Osservatorio Astronomico di Torino. We wish to thank V. Springel for kindly providing us with his code GADGET, and Martina Giovalli which implemented the simple star formation prescription in it. We thank the referee for his suggestions, useful to improve the paper.

References

- Alard, C. 2001, *A&A*, 379, L44
- Avilez, M. A., Ballesteros-Paredes, J., & Mac Low, M.-M. 2000, in *Bulletin of the American Astronomical Society*, Vol. 32, *Bulletin of the American Astronomical Society*, 711–+
- Berentzen, I., Heller, C. H., Shlosman, I., & Fricke, K. J. 1998, *MNRAS*, 300, 49
- Bett, P., Eke, V., Frenk, C. S., et al. 2007, *MNRAS*, 376, 215
- Bournaud, F., Combes, F., & Semelin, B. 2005, *MNRAS*, 364, L18
- Combes, F. & Melchior, A. L. 2002, *Ap&SS*, 281, 383
- Combes, F. & Sanders, R. H. 1981, *A&A*, 96, 164
- Curir, A., Mazzei, P., & Murante, G. 2006, *A&A*, 447, 453
- Curir, A., Mazzei, P., & Murante, G. 2007, *ArXiv Astrophysics e-prints*
- Friedli, D. & Benz, W. 1995, *A&A*, 301, 649
- Katz, N., Weinberg, D. H., & Hernquist, L. 1996, *ApJS*, 105, 19
- Klypin, A., Kravtsov, A. V., Bullock, J. S., & Primack, J. R. 2001, *ApJ*, 554, 903

- Maller, A. H., Dekel, A., & Somerville, R. 2002, MNRAS, 329, 423
Martinet, L. & Friedli, D. 1997, A&A, 323, 363
Mazzei, P. & Curir, A. 2001, A&A, 372, 803
Mazzei, P. & Curir, A. 2003, ApJ, 591, 784
Michel-Dansac, L. & Wozniak, H. 2006, A&A, 452, 97
Navarro, J. F., Frenk, C. S., & White, S. D. M. 1996, ApJ, 462, 563
Navarro, J. F., Frenk, C. S., & White, S. D. M. 1997, ApJ, 490, 493
Press, W. H., Flannery, B. P., & Teukolsky, S. A. 1986, Numerical recipes. The art of scientific computing (Cambridge: University Press, 1986)
Robertson, B., Yoshida, N., Springel, V., & Hernquist, L. 2004, ApJ, 606, 32
Rosen, A. & Bregman, J. N. 1995, ApJ, 440, 634
Semelin, B. & Combes, F. 2002, A&A, 388, 826
Springel, V. 2005, MNRAS, 364, 1105
Springel, V. & Hernquist, L. 2003, MNRAS, 339, 289
Tasker, E. J. & Bryan, G. L. 2006, ApJ, 641, 878
Wada, K. 2001, ApJ, 559, L41
Wada, K. & Norman, C. A. 2001, ApJ, 547, 172
Wechsler, R. H., Bullock, J. S., Primack, J. R., Kravtsov, A. V., & Dekel, A. 2002, ApJ, 568, 52